PHYSICAL REVIEW B **90**, 220511(R) (2014)

Current inversion at the edges of a chiral *p*-wave superconductor

Adrien Bouhon* and Manfred Sigrist
Institute for Theoretical Physics, ETH Zurich, Zurich, Switzerland

(Received 4 September 2014; revised manuscript received 26 November 2014; published 22 December 2014)

Motivated by Sr_2RuO_4, edge quasiparticle states are analyzed based on the self-consistent solution of the Bogolyubov–de Gennes equations for a topological chiral p-wave superconductor. Using a tight-binding model of a square lattice for the dominant γ band, we explore the nontrivial geometry and band structure dependence of the edge states and currents. As a peculiar finding, we show that, for high band fillings, currents flow in a reversed direction when comparing straight and zigzag edges. We give a simple explanation in terms of the positions of the zero-energy bound states using a quasiclassical picture. We also show that a Ginzburg-Landau approach can reproduce these results. Moreover, the band filling dependence of the most stable domain wall structure is discussed.

DOI: 10.1103/PhysRevB.90.220511 PACS number(s): 74.20.Pq, 74.20.De, 74.25.fc, 74.70.Pq

Since the discovery of superconductivity in Sr_2RuO_4, numerous experiments have revealed the unconventional nature of the pairing state, with many suggesting the spin-triplet chiral p-wave (CPW) state as the strongest candidate [1–3]. This state belongs to the two-dimensional irreducible representation E_u of the tetragonal point group (D_{4h}) with a gap function parametrized by the vector $\boldsymbol{d}(\boldsymbol{k}) = -\mathrm{tr}\{\hat{\Delta}_{\boldsymbol{k}} i\hat{\sigma}_y \hat{\boldsymbol{\sigma}}\}/2 = \hat{z}\Delta_0(k_x \pm ik_y)/k_F$, where $\hat{\Delta}_{\boldsymbol{k}}$ is the gap matrix in spin space and Δ_0 is the gap magnitude [4,5]. It was pointed out that chiral superconducting phases are topological superconducting phases which can be characterized through the topological invariant associated with their ground states [6–10]. Since time reversal symmetry is broken, the topology is distinguished by the Chern number ($C_1 \in \mathbb{Z}$).

An important consequence of the topology is that spatial defects (sample surfaces, domain walls, etc.), where the Chern number changes, can host quasiparticle bound states whose energy eigenvalues cross the energy gap and connect the two separate sectors of the bulk spectrum. Generally, in a chiral phase such a gap crossing yields an imbalance between certain momentum directions along the defect such that the bound states can generate a quasiparticle flow and local currents. In particular, in a CPW state we expect such surface currents to generate local magnetic fields. While edge states have been observed by tunneling spectroscopy in Sr_2RuO_4 [11], attempts to observe chiral edge currents have failed so far [12–14]. Our aim is to shed light on this question based on a microscopic study of the edge states in the CPW state.

Using a tight-binding model of a square lattice for the γ band of Sr_2RuO_4 [15] and, assuming a CPW state, we solve the Bogolyubov–de Gennes (BdG) equations self-consistently. We study the geometry and band structure dependence of the edge states and discuss the current pattern that they generate. It turns out that edge states and currents can strongly depend on the band filling and the orientation of the surfaces. For certain conditions the edge state spectrum qualitatively changes and reverses the edge current directions and can give rise to an unusual current pattern. This modification can also be straightforwardly reproduced within a Ginzburg-Landau formulation.

*abouhon@phys.ethz.ch

The effective tight-binding mean field Hamiltonian reads

$$\mathcal{H} = \sum_{ij} \epsilon_{ij} c_i^\dagger c_j + \Delta_{ij} c_i^\dagger c_j^\dagger + \Delta_{ji}^* c_i c_j, \tag{1}$$

where $\epsilon_{ij} = (\epsilon_0 - \mu)\delta_{ij} - t_\gamma \delta_{\langle ij\rangle} - t'_\gamma \delta_{\langle\langle ij\rangle\rangle}$ is the tight-binding dispersion relation of the γ band with on-site $(\epsilon_0 - \mu)$, nearest-neighbor (t_γ), and next-to-nearest-neighbor (t'_γ) hopping terms. The mean field gap function is defined through the gap equation $\Delta_{ij} = -g_{ij}\langle c_i c_j\rangle$, with the pairing $g_{ij} = g^p \delta_{\langle ij\rangle}$, where we restrict to nearest-neighbor (intersublattice) pairing interactions. The homogeneous system follows the Hamiltonian,

$$\mathcal{H}^{\mathrm{bulk}} = \sum_{\boldsymbol{k}} \boldsymbol{c}_{\boldsymbol{k}}^\dagger h_{\boldsymbol{k}} \boldsymbol{c}_{\boldsymbol{k}}, \quad h_{\boldsymbol{k}} = \begin{bmatrix} \epsilon_{\boldsymbol{k}} & \Delta_{\boldsymbol{k}} \\ \Delta_{\boldsymbol{k}}^* & -\epsilon_{\boldsymbol{k}} \end{bmatrix}, \tag{2}$$

with $\boldsymbol{c}_{\boldsymbol{k}} = (c_{\boldsymbol{k}} c_{-\boldsymbol{k}}^\dagger)^T$. The dispersion relation for the γ band is now given by $\epsilon_{\boldsymbol{k}} = \epsilon_0 - \mu - 2t_\gamma(\cos k_x a + \cos k_y a) - 4t'_\gamma \cos k_x a \cos k_y a$, and the gap function is $\Delta(\boldsymbol{k}) = \Delta_x \sin k_x a + \Delta_y \sin k_y a$, with $(\Delta_x, \Delta_y) = \Delta_0(1, \pm i)$ ($\Delta_0 \in \mathbb{R}$).

In the following we solve the Bogolyubov–de Gennes equation for a ribbon shaped system based on the Hamiltonian (1) for two basic orientations: one parallel to a principal crystal direction having straight edges, and the other along the diagonal direction, with zigzag edges. We assume translational invariance and impose periodic boundary conditions along the ribbon direction, introducing the Bloch wave vector parallel to the edge, $k_\parallel$, to label the eigenstates and energy eigenvalues. For a ribbon with N sites in the perpendicular direction we then have N equations,

$$\sum_j \begin{bmatrix} \epsilon_{ij}(k_\parallel) & \Delta_{ij}(k_\parallel) \\ \Delta_{ji}^*(k_\parallel) & -\epsilon_{ij}(-k_\parallel) \end{bmatrix} \begin{bmatrix} u_{j,k_\parallel}^n \\ v_{j,k_\parallel}^n \end{bmatrix} = E_{n,k_\parallel} \begin{bmatrix} u_{i,k_\parallel}^n \\ v_{i,k_\parallel}^n \end{bmatrix}, \tag{3}$$

which lead to a spectrum of $2N$ eigenvalues $\{E_{n,k_\parallel}\}_{n=1,\ldots,2N}$ for every $k_\parallel$ belonging to the reduced Brillouin zone $(-\Lambda_\parallel, \Lambda_\parallel]$. The local spectral function is then given by

$$A(E, k_\parallel, \boldsymbol{r}_i) = \sum_{n=1}^{2N} \left|u_{i,k_\parallel}^n\right|^2 \delta(E - E_{n,k_\parallel}). \tag{4}$$

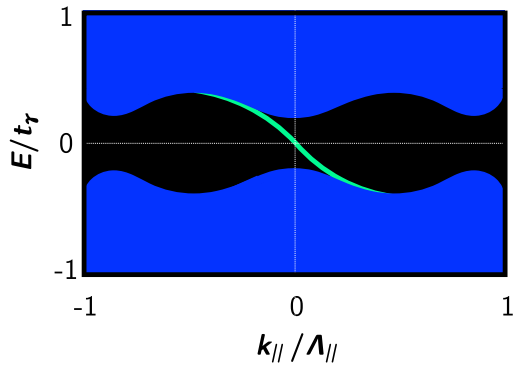

(a) $\theta_{\mathrm{Edge}} = 0^{\circ}$.

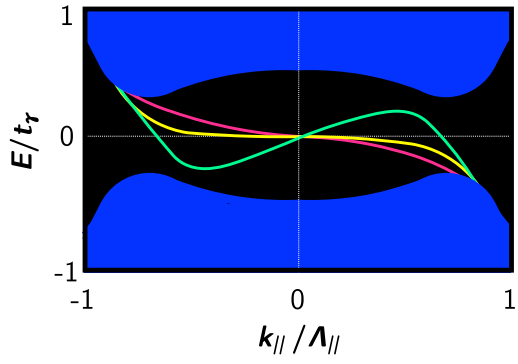

(b) $\theta_{\mathrm{Edge}} = 45^{\circ}$.

FIG. 1. (Color online) Spectral function (drawing made from the numerical self-consistent solution of the BdG equation) at an edge of a ribbon as a function of the Block wave vector parallel to the edge, $k_{\parallel} \in (-\Lambda_{\parallel}, \Lambda_{\parallel}]$, and the quasiparticle energy E. The coordinates are chosen such that the normal vector at the surface $\boldsymbol{n} = (1,0,0)$ is pointing outwards. (a) Straight edge, i.e., the angle of the edge with respect to the main crystal direction, is $\theta_{\mathrm{edge}} = 0^{\circ}$. (b) Zigzag edge, i.e., with $\theta_{\mathrm{edge}} = 45^{\circ}$, at different fillings: low filling (red line), high filling (green line), and transition filling (yellow line).

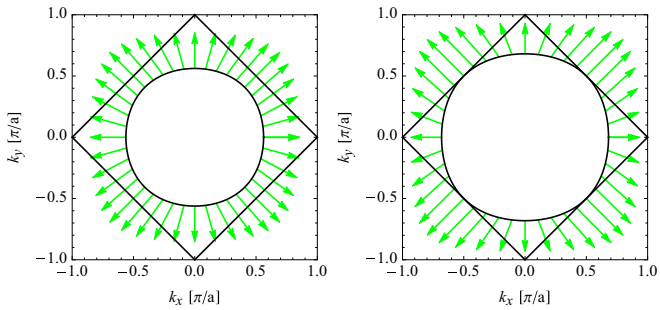

(a) $\mu - \epsilon_0 < 0$. (b) $\mu - \epsilon_0 = 0$.

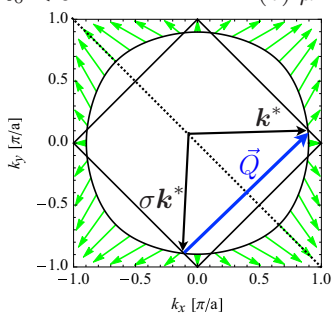

(c) $\mu - \epsilon_0 > 0$.

FIG. 2. (Color online) CPW gap function of the γ band at the Fermi level, $\Delta(\boldsymbol{k}_F)/\Delta_0 = \sin k_{F,x}a + i \sin k_{F,y}a$, represented as a vector in the complex plane $(k_x, ik_y) \in \mathbb{C}$, for different fillings. (a) Low filling: There is no crossing point between the Fermi surface and the nesting diamond. (b) Transition filling: The Fermi surface touches the nesting diamond. (c) High filling: There are four pairs of crossing points between the Fermi surface and the nesting diamond, which we write $\boldsymbol{k}^*$. We note that in addition to the π-phase shift of the gap function under inversion, at high filling there is a π-phase shift of the gap function between each two crossing points $\boldsymbol{k}^*$ and $\sigma\boldsymbol{k}^*$, where σ is the reflection operation for a mirror plane along the diagonal of the Brillouin zone. They are connected through $\boldsymbol{k}^* = \sigma\boldsymbol{k}^* + \boldsymbol{Q}$, with the "nesting" vector $\boldsymbol{Q} = (\pi/a, \pi/a)$.

The clearest signature of the topological nature of the superconducting state can be seen in the edge states, as displayed in Fig. 1 through the local spectral function at one edge of the ribbon. Figure 1(a) shows the situation for the straight edge ($\theta_{\mathrm{edge}} = 0^{\circ}$) with one spin degenerate subgap edge mode crossing from the upper to the lower continuum. The qualitative behavior does not depend on band filling. This is different for the case of the zigzag edge ($\theta_{\mathrm{edge}} = 45^{\circ}$), where an intriguing filling dependence can be observed in Fig. 1(b). The three subgap spectra correspond to the fillings depicted in Fig. 2. For small filling the Fermi surface lies within the "nesting" diamond [Fig. 2(a)] and the CPW state generates a spectrum analogous to the case of Fig. 2(a) with one zero crossing of the edge state (red curve). On the other hand, if the band crosses the diamond [Fig. 2(c)], then we find three momenta $k_{\parallel}$ with zero-energy states (green curve). The transition between the two limits is continuous where the subgap state energy dispersion is flat at the crossing point $k_{\parallel} = 0$ (yellow curve), coinciding with the band filling for which the Fermi surface just touches the diamond [Fig. 2(b)].

The unexpected behavior for the large band filling (green curve in Fig. 1) is caused by the phase structure of the gap function on the Fermi surface plotted in Fig. 2(c). It is straightforward to derive from a quasiclassical approach that a phase shift of π of the gap function between the momenta incident to the edge and scattered from the edge, $\boldsymbol{k}$ and $\boldsymbol{k}' = \sigma\boldsymbol{k}$, with σ being the reflection operation using a mirror plane parallel to the sample edge (for specular scattering), leads to the existence of a zero-energy state with the momentum $\boldsymbol{k}_{\parallel} = (\boldsymbol{k} + \boldsymbol{k}')/2$.

The gap function based on nearest-neighbor pairing acquires a π-phase shift for straight edges, generally, and zigzag edges at small filling [Fig. 2(a)] only, if $k_{\parallel} = 0$. The crossing points of the Fermi surface on the nesting diamond in Fig. 2(c) play a special role for the zigzag edge, because they correspond to momenta with $\boldsymbol{k}' - \boldsymbol{k} = \boldsymbol{Q} = (\pi/a, \pi/a)$, where we find for intersublattice pairing $\Delta(\boldsymbol{k}') = \Delta(\boldsymbol{k} + \boldsymbol{Q}) = -\Delta(\boldsymbol{k})$, i.e., for these momenta also a π-phase difference appears, leading to additional zero-energy states.

It is important to notice that this modification of the spectrum is not a topological feature. The topology of the superconducting phase is described by the Chern number given

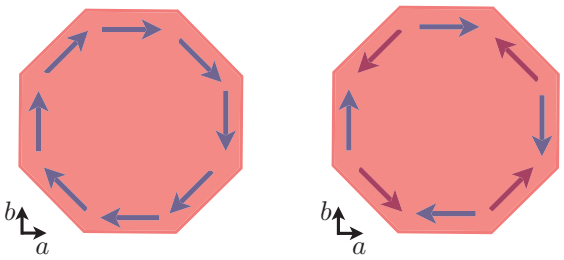

(a) Low filling. (b) High filling.

FIG. 3. (Color online) Schematic edge current pattern for an octagonally shaped sample at (a) low and (b) high filling. If it is a CPW superconductor, Sr_2RuO_4 belongs to the regime (b).

by the integral

$$C_1 = \frac{1}{4\pi}\int_{T^2} d^2k \hat{m}_{\boldsymbol{k}} \cdot \left(\partial_{k_x}\hat{m}_{\boldsymbol{k}} \times \partial_{k_y}\hat{m}_{\boldsymbol{k}}\right), \tag{5}$$

where the bulk Hamiltonian (2) is represented as $h_{\boldsymbol{k}} = \boldsymbol{m}_{\boldsymbol{k}} \cdot \hat{\boldsymbol{\sigma}}$, from which we obtain the unit vector $\hat{m}_{\boldsymbol{k}} = \boldsymbol{m}_{\boldsymbol{k}}/|\boldsymbol{m}_{\boldsymbol{k}}|$. The difference in the Chern numbers on the two sides of the edge, i.e., sample and vacuum, coincides with the number of states in the spectrum traversing from the upper to the lower bulk continuum when scanning the $k_\parallel$ from $-\Lambda_\parallel$ to $+\Lambda_\parallel$. In our case, $\Delta C_1 = C_1(\text{outside}) - C_1(\text{inside}) = 0 - 1 = -1$ implies that one state moves down, as can be seen in Figs. 1(a) and 1(b). Indeed, this feature remains unchanged even in the case of three zero crossings.

We add here a remarkable observation concerning the current density at different edges. To motivate this we analyze qualitatively the contribution of the subgap bound states to the edge current density, which we express as $J_\parallel \propto \sum_{k_\parallel} n_{k_\parallel} v_{k_\parallel}$. Note that the velocity $v_{k_\parallel}$ is determined by the quasiparticle dispersion at the Fermi surface and $v_{-k_\parallel} = -v_{k_\parallel}$. For $T = 0$ only states with negative energy have $n_{k_\parallel} \neq 0$. For straight edges these are only bound states with $k_\parallel > 0$ for all band fillings, as is obvious from Fig. 1(a). On the other hand, for zigzag edges we see a change in the momentum distribution. While for small filling the situation is identical to the straight edge, for large filling the distribution of the occupied edge states shifts to negative $k_\parallel$ [Fig. 1(b)]. From this simple discussion we anticipate a reversal of the current density for zigzag edges at high filling, since the Fermi surface topology is unchanged (Fig. 2) and $v_{k_\parallel}$ keeps its momentum dependence qualitatively over the range of band filling considered here. This qualitative observation is indeed confirmed by our detailed numerical analysis including all contributions the edge currents. By interpolation we can state that the edge current density has to vanish at an intermediate orientation, i.e., for $0 < \theta e < 45^\circ$, in this case.

It is illustrative to plot schematically the edge current patterns in an octagonally shaped sample corresponding to the low- and high-filling regimes in Figs. 3(a) and 3(b), respectively. While at low filling the edge current has a fully connected current circuit analogous to the quantum Hall state, at high filling the edge current now alternates between the straight and zigzag edges. In the latter case the overall current pattern would be somewhat more complex. Note, however, that edge currents are compensated over a distance of London penetration depth so as to screen the induced magnetic fields. The filling for Sr_2RuO_4 is rather large—a typical estimate for the γ band is $(\mu - \epsilon_0)/t_\gamma \approx 1.4$ [16]. Thus, if it realizes the CPW state, we expect this material to most likely exhibit the edge current pattern of Fig. 3(b).

We now turn to the Ginzburg-Landau (GL) formulation which also accounts for edge currents. The GL free energy functional can be expanded in the two complex order parameter components (Δ_x, Δ_y) belonging to the irreducible representation E_u of the point group D_{4h}. We focus here on the gradient terms of the free energy density, needed to express the current density,

$$f_{\text{grad}} = \sum_{\mu,\nu=x,y} [K_{\mu\nu}|\Pi_\mu \Delta_\nu|^2 + \tilde{K}_{\mu\nu}\{(\Pi_\mu \Delta_\nu)^*(\Pi_{\bar{\mu}}\Delta_{\bar{\nu}}) + \text{c.c.}\}], \tag{6}$$

with $\Pi_\mu = \frac{\hbar}{i}\partial_\mu + \gamma A_\mu$ $(\gamma = 2e/c)$, A_μ the vector potential, and $(\bar{x}, \bar{y}) = (y, x)$ [17]. Within a weak-coupling approach for our tight-binding model we derive the coefficients $K_{\mu\nu}$ and $\tilde{K}_{\mu\nu}$. These are given by the following averages over the Fermi surface, $K_{\mu\nu} = K_0\langle N_0 v_{F\mu}^2 \phi_\nu^2\rangle_{\text{FS}}$ and $\tilde{K}_{\mu\nu} = K_0\langle N_0 v_{F\mu} v_{F\bar{\nu}} \phi_\nu \phi_{\bar{\mu}}\rangle_{\text{FS}}$, with K_0 a common constant. The density of states is given by $N_0(\boldsymbol{k}) \propto |\boldsymbol{k}_F|/|\boldsymbol{v}_F|$, the Fermi velocities are defined as $\boldsymbol{v}_F = \nabla_k \epsilon(\boldsymbol{k})|_{\boldsymbol{k}=\boldsymbol{k}_F}$, and the gap lattice form factors are given by $\phi_\nu = \sin k_\nu a$ for nearest-neighbor pairing. Note that by symmetry, $K_{xx} = K_{yy}$, $K_{xy} = K_{yx}$, $\tilde{K}_{xx} = \tilde{K}_{yy} = \tilde{K}_{xy} = \tilde{K}_{yx}$, and all coefficients are positive.

We consider now the edge currents within the GL formulation. The order parameter at the edge can be characterized by the simplified boundary conditions (ignoring the vector potential) that the component $\Delta_n = 0$ and $\partial_n \Delta_{\bar{n}} = 0$ at the surface, where n denotes the component perpendicular ($\bar{n}$ parallel) and ∂_n is the derivative perpendicular to the surface. We restrict ourselves to the two main directions with $\theta_{\text{edge}} = 0^\circ$ and 45°. An approximative spatial dependence of the order parameter is given by $\Delta_n(r_n) = \Delta_0 \tanh(-r_n/\xi_n)$ and $\Delta_{\bar{n}} = i\Delta_0$, with $r_n < 0$ the coordinate perpendicular to the surface located at $r_n = 0$ and ξ_n the corresponding healing length. The current density j_n perpendicular to the surface vanishes naturally and the current density parallel is approximately given by

$$j_{\bar{n}}(r_n) \propto K_n \Delta_0 \partial_n |\Delta_n(r_n)| = -\frac{K_n \Delta_0^2}{\xi_n}\cosh^{-2}(r_n/\xi_n), \tag{7}$$

where $K_n = \tilde{K}_{xx}$ for $\theta_{\text{edge}} = 0^\circ$ and $K_n = (K_{xx} - K_{xy})/2$ for $\theta_{\text{edge}} = 45^\circ$. Therefore, we always find a negative current density along a straight right edge [since $\partial_n|\Delta_n(r_n)|_{r_n=0} < 0$]. On the other hand, the sign of the current density parallel to a zigzag edge depends on the ratio K_{xx}/K_{xy}. Using the weak-coupling expressions of the GL coefficients, we plot this ratio in Fig. 4 as a function of the filling $\mu - \epsilon_0$ (the other tight-binding parameters are kept constant). We find a threshold filling μ_c above which the ratio K_{xx}/K_{xy} becomes smaller than 1, leading to a positive current density parallel to a zigzag edge (the other way around if the filling is below μ_c). Therefore, when $\mu < \mu_c$, the profile of the GL edge currents of an octagonal sample corresponds to Fig. 3(a), and when $\mu > \mu_c$, it is given by Fig. 3(b). The full self-consistent solution of the quasiclassical and Ginzburg-Landau equations

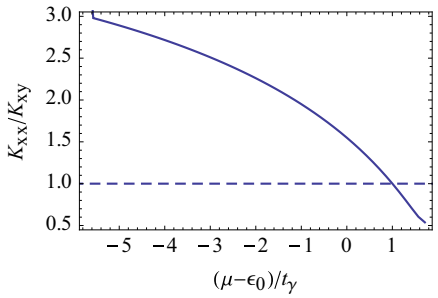

FIG. 4. (Color online) Ratio of Ginzburg-Landau coefficients K_{xx}/K_{xy} as a function of the filling $\mu-\epsilon_0$, computed in the weak-coupling limit for a tight-binding model. The remaining tight-binding parameter is chosen as $t'_\gamma/t_\gamma = 0.43$. There is a threshold filling, $(\mu_c-\epsilon_0)/t_\gamma \approx 1$, above which K_{xy} is bigger than K_{xx}. At $(\mu-\epsilon_0)/t_\gamma = -5.71$, the filling is zero (isotropic limit) with the ratio $K_{xx}/K_{xy} = 3$.

for the straight and zigzag edges will be presented in a future publication.

We briefly address here the consequences of the filling dependence of the ratio K_{xx}/K_{xy} for the structure of domain walls in the CPW state, parallel to one principal crystal axis, i.e., $\theta_{\rm DW} = 0$. An approximate shape of the domain wall can be given by $\Delta_\nu(x) = \alpha_\nu \Delta_0 \tanh(x/\tilde{\xi})$ and $\Delta_{\bar{\nu}} = \beta_{\bar{\nu}}\Delta_0$, with $\tilde{\xi} \propto \sqrt{K_{xv}}$, $(\alpha_x,\beta_y) = (1,i)$, and $(\alpha_y,\beta_x) = (i,1)$ for the two basic structures. Inserting this into the GL free energy, we obtain $E_{\rm DW} \propto \tilde{\xi} \propto \sqrt{K_{xv}}$, such that the relative energy between the two types of domain wall is simply given by the ratio K_{xx}/K_{xy}. The stable domain wall structure (for $\theta_{\rm DW} = 0$) is once more determined by the band filling. When $\mu < \mu_c$, the domain wall has a kink in the parallel component, here Δ_y, and when $\mu > \mu_c$, the most stable domain wall has a kink in the perpendicular component, here Δ_x. Discussions of stable domain wall shapes have so far been based on the low-filling properties of the CPW. Our extension here requires, therefore, also a revision of the conclusions drawn based on domain wall structure, in particular, in the context of interference effects in Josephson contacts [18–21].

Finally, let us comment on a recent experiment aiming at detecting edge currents by a scanning magnetometer on the top surface of small cylinders (of radius $r \sim 5$–$10\ \mu$m) of a highly pure single crystal of Sr_2RuO_4 [14]. Since our analysis of a CPW state that is compatible with the γ band of Sr_2RuO_4 reveals the reversal of current flow between the straight and zigzag edges [Fig. 3(b)], we expect that the edge currents may be strongly suppressed in circularly shaped samples of small radius. This might be responsible for the rather small upper bound for the currents, stated by Ref. [14]. Obviously, also currents at extended edges might be influenced by our finding, in particular, if the edges are faceted and lead to retroreflection [12,22,23]. Note that a perfectly square sample might be more suitable for a stronger conclusion.

We conclude by noting that functional renormalization group calculations suggest that next-to-nearest-neighbor pairing terms are very important in Sr_2RuO_4 [15]. Introducing them does not change the qualitative picture discussed in this work as long as the nearest-neighbor pairing coupling dominates. With growing next-to-nearest-neighbor pairing, the CPW state exhibits a phase transition from the topological sector $C_1 = \pm 1$ to $C_1 = \mp 3$ as a function of the filling. While the qualitative picture for the edge currents and our basic conclusions remain unchanged through such a transition, the bound state spectrum is strongly modified. A detailed discussion corresponding to this situation will be discussed elsewhere [24].

We are grateful to S. Etter, G. M. Graf, Y. Imai, and T. M. Rice for many helpful discussions. This study has been financially supported by the Swiss National Science Foundation.

[1] A. P. Mackenzie and Y. Maeno, Rev. Mod. Phys. **75**, 657 (2003).
[2] Y. Maeno, T. M. Rice, and M. Sigrist, Phys. Today **54**(1), 42 (2001).
[3] Y. Maeno, S. Kittaka, T. Nomura, S. Yonezawa, and K. Ishida, J. Phys. Soc. Jpn. **81**, 011009 (2012).
[4] R. Balian and N. R. Werthamer, Phys. Rev. **131**, 1553 (1963).
[5] A. J. Leggett, Rev. Mod. Phys. **47**, 331 (1975).
[6] A. V. Balatsky, G. E. Volovik, and V. A. Konyshev, Zh. Eksp. Teor. Fiz. **90**, 2038 (1986) [Sov. Phys. JETP **63**, 1194 (1986)].
[7] G. E. Volovik, *Exotic Properties of Superfluid ^3He* (World Scientific, Singapore, 1992).
[8] G. E. Volovik, JETP Lett. **66**, 522 (1997).
[9] G. E. Volovik, *The Universe in a Helium Droplet* (Oxford University Press, Oxford, UK, 2003).
[10] A. Furusaki, M. Matsumoto, and M. Sigrist, Phys. Rev. B **64**, 054514 (2001).
[11] S. Kashiwaya, H. Kashiwaya, H. Kambara, T. Furuta, H. Yaguchi, Y. Tanaka, and Y. Maeno, Phys. Rev. Lett. **107**, 077003 (2011).
[12] J. R. Kirtley, C. Kallin, C. W. Hicks, E.-A. Kim, Y. Liu, K. A. Moler, Y. Maeno, and K. D. Nelson, Phys. Rev. B **76**, 014526 (2007).
[13] J. Jang, D. G. Ferguson, V. Vakaryuk, R. Budakian, S. B. Chung, P. M. Goldbard, and Y. Maeno, Science **331**, 186 (2011).
[14] P. J. Curran, S. J. Bending, W. M. Desoky, A. S. Gibbs, S. L. Lee, and A. P. Mackenzie, Phys. Rev. B **89**, 144504 (2014).
[15] Q. H. Wang, C. Platt, Y. Yang, C. Honerkamp, F. C. Zhang, W. Hanke, T. M. Rice, and R. Thomale, Europhys. Lett. **104**, 17013 (2013).
[16] C. Bergemann, A. P. Mackenzie, S. R. Julian, D. Forsythe, and D. Ohmichi, Adv. Phys. **52**, 639 (2003).
[17] M. Sigrist and K. Ueda, Rev. Mod. Phys. **63**, 239 (1991).
[18] F. Kidwingira, J. D. Strand, D. J. Van Harlingen, and Y. Maeno, Science **314**, 1267 (2006).
[19] D. Bahr, Ph.D. dissertation, University of Illinois, 2011.
[20] M. S. Anwar *et al.*, Sci. Rep. **3**, 2480 (2013).
[21] A. Bouhon and M. Sigrist, New J. Phys. **12**, 043031 (2010).
[22] J. A. Sauls, Phys. Rev. B **84**, 214509 (2011).
[23] S. Lederer, W. Huang, E. Taylor, S. Raghu, and C. Kallin, Phys. Rev. B **90**, 134521 (2014).
[24] A. Bouhon and M. Sigrist (unpublished).